Deformation Behavior of Polyethylene/Silicate Nanocomposites As Studied by Real-Time Wide-Angle X-ray Scattering

Ki Hyun Wang,[†] In Jae Chung,*[,†] Min Cheol Jang,[‡] Jong Kahk Keum,[‡] and Hyun Hoon Song*[,‡]

Department of Chemical Engineering, Korea Advanced Institute of Science and Technology, 373-1, Kusong-dong, Yusong-gu, Daejeon 305-701, South Korea, and Department of Polymer Science and Engineering, Hannam University, 133, Ojung-dong, Daeduk-gu, Daejeon 306-791, South Korea

Received February 1, 2002

ABSTRACT: Maleated polyethylene/silicate nanocomposite (PEMA/20A) and maleated polyethylene/SiO_2 composite (PEMA/SiO_2) were prepared by the melt compounding. Transmission electron microscopy and X-ray scattering results confirmed the exfoliation of the silicate layers (20A) throughout the maleated polyethylene (PEMA) matrix, but the SiO_2 particles were not well dispersed in the matrix. The long axes of exfoliated silicates were aligned along the tensile axis during deformation and showed no sign of cavity formation in the matrix. In PEMA/SiO_2, however, extensive amount of cavities were created along the tensile direction. During the tensile deformation the crystallographic changes of pure PEMA and composites containing 20A and SiO_2 were investigated using the real-time X-ray scattering. The 20A and SiO_2 particles in composites made little effects on the initiation of martensitic transformation, but they effectively inhibited the orientation of polyethylene lamellae in the tensile direction. The lamellar fragmentation was higher in PEMA/20A than in PEMA/SiO_2, while the former was less effective in inhibiting lamellar orientation.

Introduction

Polymer nanocomposites are a class of hybrid materials composed of an organic polymer matrix in which inorganic particles of nanoscale dimensions are imbedded.[1−6] The inorganic fillers dispersed well in the polymer matrix improve dramatically the mechanical properties of the nanocomposite even though their amount is small. The polymer nanocomposites also exhibit other various enhanced properties including high heat distortion temperature, enhanced flame resistance, better barrier property, and decreased thermal expansion coefficient.[7,8] The enhanced properties are presumably due to the synergistic effects of the nanoscale structure and the maximized interaction between the fillers and polymer molecules.

The enhanced properties of nanocomposites have attracted extensive research interest in polymer/silicate nanocomposites in recent years.[9] The melt intercalation method to produce the nonpolar polymer/silicate nanocomposites is based on the introduction of an organic modifier to mediate the polarity between the hydrophilic silicate surface and the hydrophobic polymer.[10−18]

One of the typical examples is the polypropylene/silicate nanocomposite system suggested by Toyota.[17] In polyethylene, which is nonpolar, homogeneous dispersion of hydrophilic silicate layers cannot be realized without maleic anhydride modification. The role and effect of maleic anhydride in preparation of polyolefin nanocomposites has already been well described.[19]

Although research efforts have been extensively devoted to the development of novel synthetic approaches as well as to the investigation of the physical properties in polymer nanocomposites, the microscopic mechanisms responsible for the improvement of mechanical properties have not been fully identified. To achieve a fundamental understanding of nanolayer reinforcement, there is a great need to define the exact role of nanofiller particles in the matrix and the effect of interfacial interactions between silicate layers and polymer matrix during the deformation process.

In-situ X-ray scattering upon deformation, by utilizing the very strong flux of synchrotron radiation source, has proven to be a very effective technique to examine the fine structural changes at the microscopic level and thus to provide in-depth understanding of the deformation mechanisms. Recently, several research groups have successfully conducted the real-time X-ray scattering of deforming polymers to reveal the microscopic structural changes that occur at particular points of stress−strain curve.[20−23]

In this work, we also conducted the real-time X-ray scattering study upon deforming not only the polymer nanocomposite (maleated polyethylene (PEMA) containing exfoliated silicates) but also the conventional composite (PEMA containing SiO_2 particles) and the pure PEMA. The aim of this study was to extend our current understanding of the role of the reinforcing particles in the polymer composites associated with the tensile deformation.

Experimental Section

Materials. The organically modified montmorillonite (Closite 20A; it will be called as 20A) was obtained from Southern Clay Products. 20A was the montmorillonite ion-exchanged with dimethyl dihydrogenated tallow ammonium ions, where tallow was composed predominantly of octadecyl chains with smaller amount of lower homologues. The approximate composition was C_{18} (65%), C_{16} (30%), and C_{14} (5%). Maleic anhydride modified polyethylene (PEMA) purchased from Aldrich was used as the composite matrix resin. The PEMA was linear low-density polyethylene (density = 0.930 g/cm^3) grafted with 0.85 wt % maleic anhydride. The conventional filler, SiO_2 (average particle diameter: 1.8 μm), was purchased from Fuji Sylysia.

[†] Korea Advanced Institute of Science and Technology.
[‡] Hannam University.
* To whom correspondence should be addressed: telephone 82-42-629-7504, Fax 82-42-626-8841, e-mail songhh@mail.hannam.ac.kr.

10.1021/ma020165n CCC: $22.00
Published on Web 06/04/2002

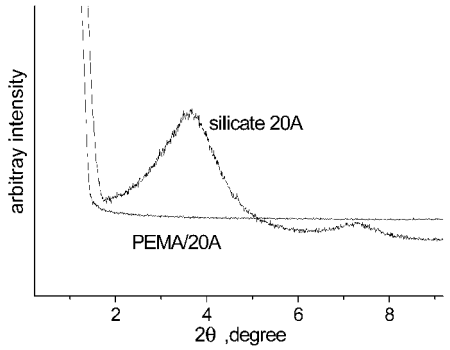

Figure 1. X-ray diffraction patterns of PEMA/20A (3 vol %) nanocomposite and pure silicate (20A).

Preparation of Composites. All composites were prepared via melt compounding at 140 °C, using a Brabender mixer with the chamber size of 50 cm^3. Screw speed was controlled at 60 rpm, and the mixing time was 20 min for each sample. The composites were then prepared into sheets by the compression molding. The samples were initially maintained at 140 °C for 5 min without applying pressure, then pressed for 10 min under a pressure of 50 bar, and successively cooled to the room temperature while maintaining the pressure.

Measurements. Transmission electron microscope (TEM) and X-ray diffraction (XRD) were used to examine the dispersion of silicates in composites before running the tensile test. XRD was carried out by using a Rigaku X-ray generator (Cu Kα radiation with $\lambda = 0.15406$ nm) at room temperature. The diffractograms were obtained at the scattering angles from 1.2° to 10° at a scanning rate of 2°/min. A transmission electron microscope, Pillips CM20, was used to observe the dispersion of silicate in composites at an acceleration voltage of 160 kV. An ultrathin section of 70 nm in thickness was prepared by an ultramicrotome, Leica EM FCS. The composite samples for tensile testing were prepared on the basis of ASTM D638 Type V. The sample thickness was 2 mm, and the distance between the grips was 25.4 mm. The samples were drawn uniaxially at the speed of 2 mm/min.

Real-Time X-ray Scattering. Real-time X-ray scattering experiments on deformation were performed at the 4C1 X-ray beam line in Pohang Accelerator Laboratory (PAL). The wavelength of synchrotron radiation source (2.5 GeV, 150 mA) was $\lambda = 1.608$ nm, and the beam size was 0.3 mm × 0.3 mm. Two-dimensional WAXS patterns were simultaneously obtained using a position-sensitive area detector while the sample was stretched at room temperature.

Results and Discussion

Preparation of Composites and Tensile Deformation. The X-ray diffraction (XRD) profiles of silicate 20A and maleated polyethylene/silicate nanocomposite (PEMA/20A) are shown in Figure 1. The (001) plane peak of 20A can be seen around $2\Theta = 3.6°$. This peak, however, disappears for the PEMA/20A nanocomposite, indicating the exfoliation of silicate in the PEMA. The transmission electron micrograph shown in Figure 2a also confirms the dispersion of 3 vol % of silicate in PEMA. The micrograph shows that each layer of silicate is well dispersed and exfoliated throughout the PEMA matrix. Dark lines in the micrograph represent the silicate layers. Figure 2b shows TEM image of maleated polyethylene/SiO_2 composite (PEMA/SiO_2) prepared in the same way as PEMA/20A. Irregular and large SiO_2 particles are observed, indicating the aggregation and poor dispersion of SiO_2 particles.

In general, the deformation behavior of semicrystalline polymers is strongly dependent on the crystallite orientation.[24−26] The morphology of a nanocomposite directly causes a remarkable difference in deformation processes, which in turn determines the ultimate macroscopic property. Figure 3 shows the tensile stress−strain curves of the composites and the pure PEMA. Three samples reveal quite different stress−strain behaviors. The composite of PEMA/20A shows the highest yield point and the pure PEMA the lowest. All three samples, on the other hand, show the double yield behavior. The first yield point locates at the similar strain, but the second yield points differ significantly between the composites and the pure PEMA. The double yielding process was first explicitly reported for branched polyethylene in 1987.[27] A typical engineering stress−nominal strain curve for a linear low-density polyethylene exhibits two maxima associated with the double yielding phenomenon as opposed to the behavior exhibited by isotropic high-density polyethylene, in which only one yield point is observed. A systematic study of double yield point in polyethylene suggested that the second yielding was enhanced as crystallinity decreased.[28] The crystallinities of PEMA/20A and PEMA/SiO_2 are similar to each other but are lower than the pure PEMA. Both PEMA/20A and PEMA/SiO_2 having a lower crystallinity than PEMA show second yield point (curves b and c in Figure 3) at lower strain than that of PEMA (curve a). The double yield and associated microscopic structural changes of the composites during the tensile deformation will be discussed further in the next section.

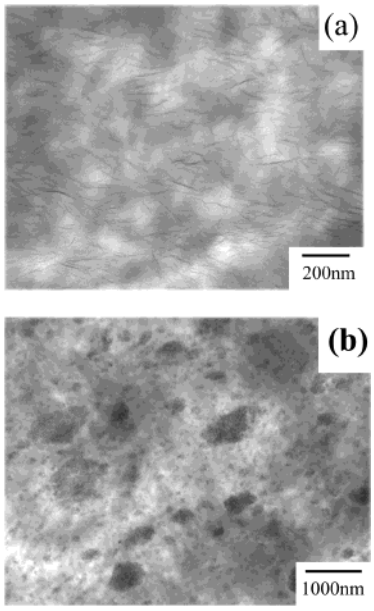

Figure 2. TEM images of composite containing 3 vol % filler: (a) PEMA/20A, (b) PEMA/SiO_2.

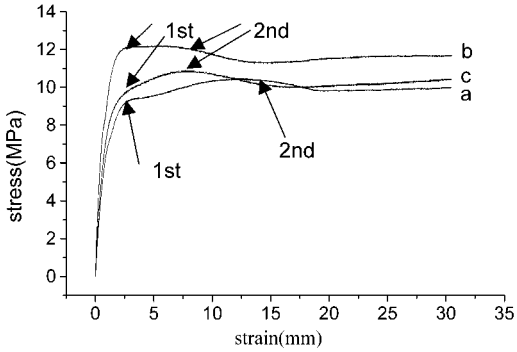

Figure 3. Stress−strain curves of composites at the strain rate of 2 mm/min: (a) PEMA, (b) PEMA/20A, (c) PEMA/SiO_2.

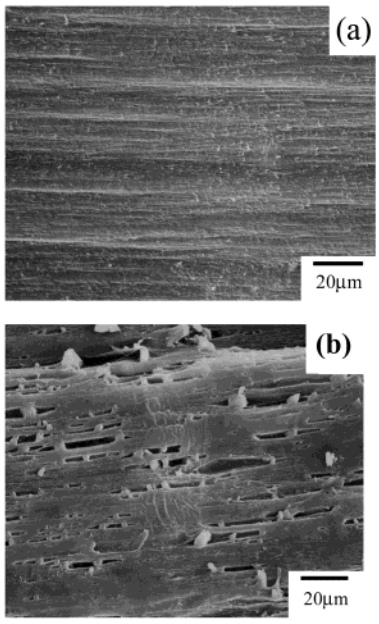

Figure 4. Scanning electron micrographs of the tensile deformed composites fractured parallel to the tensile direction: (a) PEMA/20A, (b) PEMA/SiO_2.

PEMA/20A nanocomposite shows the highest modulus and yield strength among the samples as expected, and that can be attributed to the high aspect ratio of exfoliated silicates.[29] The microstructures of the tensile deformed composites are examined by the scanning electron microscopy (SEM). Parts a and b of Figure 4 show the SEM images of PEMA/20A and PEMA/SiO_2, respectively. For SEM investigation, tensile-tested specimens frozen at the liquid nitrogen temperature were fractured in parallel to the tensile loading direction. Figure 4a shows homogeneous surface morphology without any voids in the PEMA/20A after tensile testing, demonstrating a good interfacial adhesion between the silicate and PEMA matrix. In Figure 4b, on the other hand, large and elongated cavities are seen along the load direction in the composite of conventional filler SiO_2, suggesting a poor bonding between SiO_2 and PEMA matrix. In fracture mechanics, it is known that the cavity creation in tensile deformation of composites depends on the particle size and shape as well as interfacial adhesion between the particles and matrix.[29−31] It appears that the large SiO_2 particles have played a major role in the cavitation. (In our tensile deformation of surface-modified SiO_2/PEMA, the cavitation still occurred.) But it is speculated that the poor interfacial interaction between SiO_2 and PEMA matrix also caused easy debonding upon deformation.

Real-Time X-ray Scattering Patterns with Strain. Figure 5 shows a series of WAXS patterns obtained at certain extended length of PEMA, PEMA/20A, and PEMA/SiO_2. The load direction marked with an arrow is perpendicular to the X-ray beam. Brooks et al.[33,34] have made a comprehensive study on the structural changes that occur during the double yielding behavior of isotropic polyethylene. Their results show that the first yield point signals the onset of a recoverable reorientation process of the lamellae within spherulites that leads to the final orientation of lamellae at approximately 45° to the draw direction. The second yield point is related to the destruction of these lamellae, a process related to the onset of necking and to the beginning of the spherulitic to fibrillar morphological transformation. Very intense (110) and (200) reflections for the orthorhombic structure (using $a = 7.42$ Å, $b = 4.95$ Å, $c = 2.55$ Å, $\alpha = \beta = \gamma = 90°$) are clearly visible at low strains. Additional reflections also appear during the deformation around the strain of 8−12 mm for all three samples. These new reflections can be associated with the monoclinic unit cell, indexing as $(\bar{2}01)$, (200), and (001) (using $a = 8.09$ Å, $b = 4.79$ Å, $c = 2.55$ Å, $\alpha = \beta = 90°$, and $\gamma = 107.9°$), and indicate the phase transformation called martensitic transformation induced by the stress. The (001) peak is the most intense reflection of the monoclinic cell and is clearly seen in the meridian of some patterns shown in Figure 5. Chain slip is another plastic deformation, which begins at slightly lower shear stress than the martensitic transformation.[35] The process of chain slip that causes lamellar rotation and thinning may be identified with the fine chain slip model proposed by Bowden and Young.[36] The relaxation of lamellar orientation and the martensitic transformation from the first yield point after unloading suggest reversible lamellar deformation up to this point. It appears that the first yield point is associated with the fine chain slip and the second yield point with the coarse slip, resulting in lamellar fragmentation.[20]

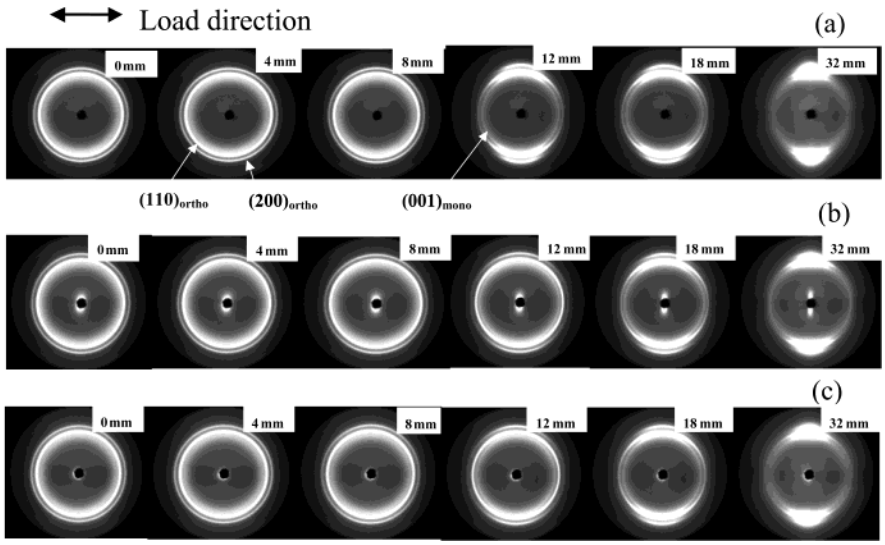

Figure 5. In-situ WAXS patterns measured during the tensile deformation: (a) PEMA, (b) PEMA/20A, (c) PEMA/SiO_2.

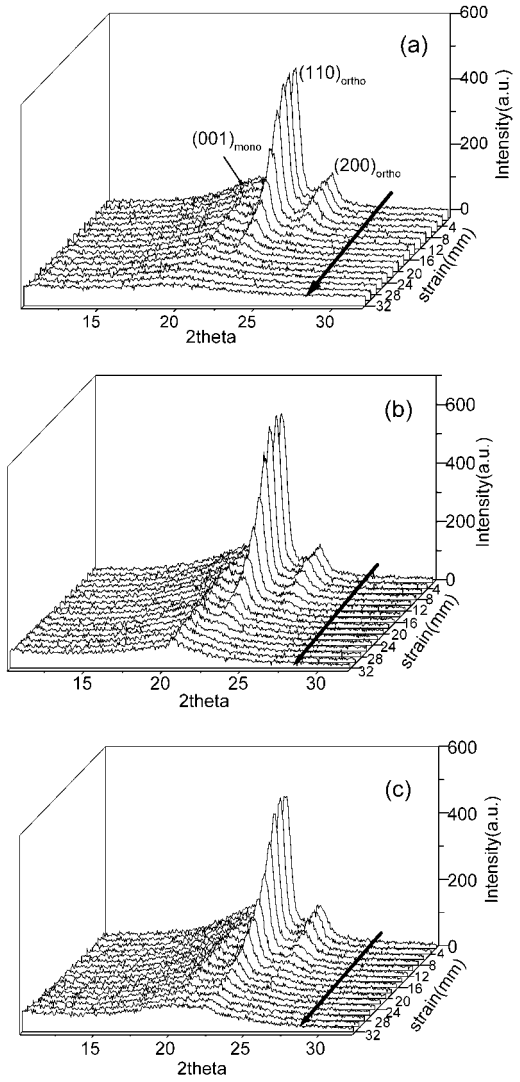

Figure 6. Meridian WAXS intensity profiles at the corresponding strains: (a) PEMA, (b) PEMA/20A, (c) PEMA/SiO_2.

The martensitic transformation shown in Figure 5 starts to appear at a higher strain than the first yield point. It seems that the onset of martensitic transformation of PEMA at a higher extension than the first yield point is associated with the branches in LLDPE[37,38] as well as with the maleic anhydride grafted to LLDPE backbone. In PEMA/20A and PEMA/SiO_2 composites the onset of martensitic transformation is even near the second yield point. It is expected that 20A and SiO_2 particles, which already showed the reduction in crystallinity of the composite matrix, also impede the martensitic transformation.

In the case of PEMA/20A the monoclinic (001) reflection is shown even at the very low strain and sustained until the large strain. But it is to be reminded that the peak near $2\Theta = 20°$ originates not only from the monoclinic (001) reflection but also from the crystallographic planes (110) and (020) of silicate layer.[39−41] Meridian intensity profiles obtained from the patterns shown in Figure 5 are plotted in Figure 6a−c. PEMA (Figure 6a) shows that the peak intensity near $2\Theta = 20°$ (monoclinic reflection) decreases and disappears at the strain of 24 mm. PEMA/SiO_2 (Figure 6c) also shows the similar behavior with that of PEMA. But in PEMA/20A (Figure 6b) the peak near $2\Theta = 20°$ still remains until the strain reaches 32 mm, which can be attributed to the additional intensity from the silicate layers.

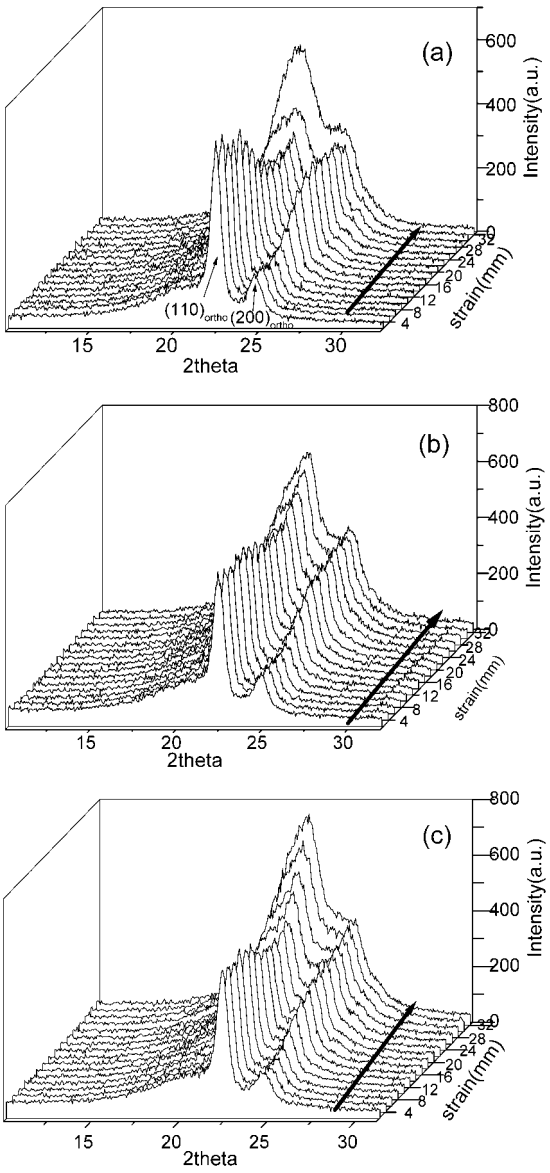

Figure 7. Equatorial WAXS intensity profiles at the corresponding strains: (a) PEMA, (b) PEMA/20A, (c) PEMA/SiO_2.

We also note a strong anisotropic scattering at the very small angle near the beam stopper in the X-ray patterns of PEMA/20A in Figure 5b. The small angle scattering pattern becomes more intense and more elongated shape with the strain. This ellipsoidal anisotropic pattern suggests the orientation of silicates during the cold drawing, as was observed in the drawn polyamide/silicate nanocomposite.[42]

Crystallographic Deformation with Strain. Figure 7 shows the evolution of scattering intensity along the equator with strain for PEMA, PEMA/20A, and PEMA/SiO_2. The orthorhombic (110) peak intensity at $2\Theta = 21.5°$ changes quite markedly for PEMA (Figure 7a). This peak intensity starts to decrease at the strain around 10 mm and then reaches a constant value until the strain reaches about 24 mm, where the peak begins to intensify again on further extension. It may be related to the molecular orientation in amorphous and crystalline region to the loading direction. We also note an extensive peak broadening at this point, demonstrating the severe fragmentation of crystalline domains.

Butler et al. showed that in polyethylene deformation the decrease in orthorhombic (110) intensity accompa-

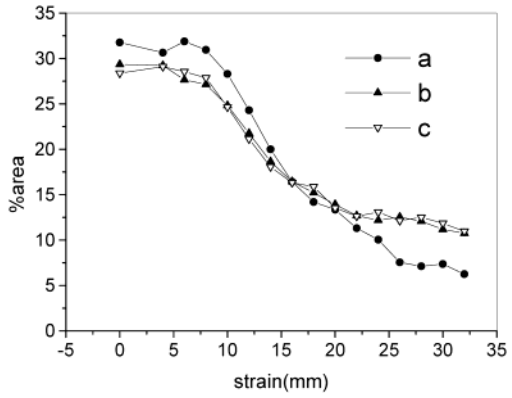

Figure 8. Changes in orthorhombic (110) peak area (%) against strain: (a) PEMA, (b) PEMA/20A, (c) PEMA/SiO_2.

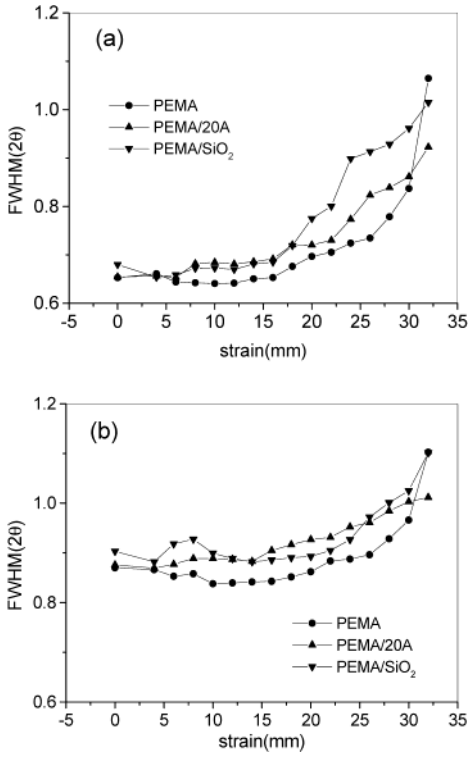

Figure 9. (a) Changes of full width at half-maximum in equatorial (110) reflection against strain. (b) Changes of full width at half-maximum in equatorial (200) reflection against strain.

nies the increase of monoclinic ($\bar{2}01$) intensity.[20] The decrease in intensity of the orthorhombic (110) peak then can be attributed to the occurrence of martensitic transformation in the sample. Figure 8 shows the changes of orthorhombic (110) peak area (%) obtained by fitting the equatorial intensity curves plotted in Figure 7. As shown in the figure, the PEMA shows the largest change in area among the samples, implying the largest degree of martensitic transformation. The greater transformation in PEMA than the other two composites may be attributed to the higher crystallinity in PEMA.[21,38] The onset of monoclinic (001) or monoclinic ($\bar{2}01$) peak appearance, however, locates at the similar strain level for all three samples.

In Figure 9a,b the full width at half-maximum (fwhm) of the orthorhombic (110) and (200) peak, obtained from the equatorial intensities in Figure 7, is plotted against the strain. The average thickness of crystallites of polyethylene decreases as the fwhm increases by the

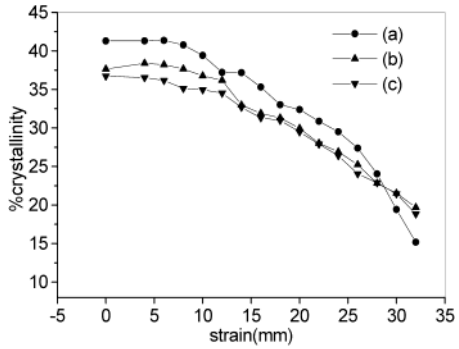

Figure 10. Plot of crystallinity as a function of strain during tensile deformation: (a) PEMA, (b) PEMA/20A, (c) PEMA/SiO_2.

Scherrer formula.[43] The second yield point marks the onset of irreversible lamellar fragmentation to fibrillar structure described by Peterlin.[44] As shown in the figures, the increment of fwhm in (110) reflections are far greater than that of (200) reflections. This means that the chain slip in polyethylene crystals, with or without filler particles, occurs preferably in the (110) planes having van der Waals interaction rather than the (200) planes of covalent bonds. As shown in Figure 9a, the fwhm of (110) in PEMA, the smallest at the early stage of deformation, increases rapidly from the strain of 26 mm and becomes the largest. However, before the strain reaches this point, PEMA shows the smallest change among the samples. It is expected that the lamellae of PEMA remain intact until the stress−strain curve reaches the plateau region after the second yield point (Figure 3) and finally fragmentation begins to occur from a certain point in the plateau region.

Even though PEMA/20A and PEMA/SiO_2 exhibit very similar behavior in (110) peak area change (Figure 8), the peak broadening observed in fwhm upon deformation is different from each other. The extent of peak broadening of PEMA/20A remains between those of PEMA and PEMA/SiO_2. PEMA/SiO_2 shows the increase in the fwhm of (110) reflection at the strain near 8 mm, which is close to the second yield point of the stress−strain curve in Figure 3. It also shows the largest increase among the samples at the plateau region of stress−strain curve (around 15 mm in strain), suggesting that the extent of fragmentation of crystal lamellae is greater in PEMA/SiO_2 than PEMA/20A. It is interesting to note that the extent of lamellae fragmentation is greater in the PEMA/SiO_2 than in the PEMA/20A nanocomposite. The higher extent of lamellae fragmentation in PEMA/SiO_2 may be associated with the cavities formed upon tensile deformation. In our previous report,[29] PEMA/SiO_2 showed the shorter elongation at break than that of PEMA/20A. It is conceived that the stress concentration on the matrix between the cavities in PEMA/SiO_2 should be high, leading to the early breakage and higher lamellae fragmentation.

Figure 10 shows the change in crystallinity of each sample, which is calculated from the sum of intensity profiles over the entire Euler anlges during the tensile process. The PEMA shows the largest reduction in crystallinity especially from the plateau region of stress−strain curve (15 mm in strain). PEMA/20A and PEMA/SiO_2 show the similar decrease in crystallinity as observed in (110) peak area changes (Figure 8). The reduction in crystallinity upon tensile deformation can be attributed to the lamellar unfolding or fragmentation associated with the chain slip. Even though the reduc-

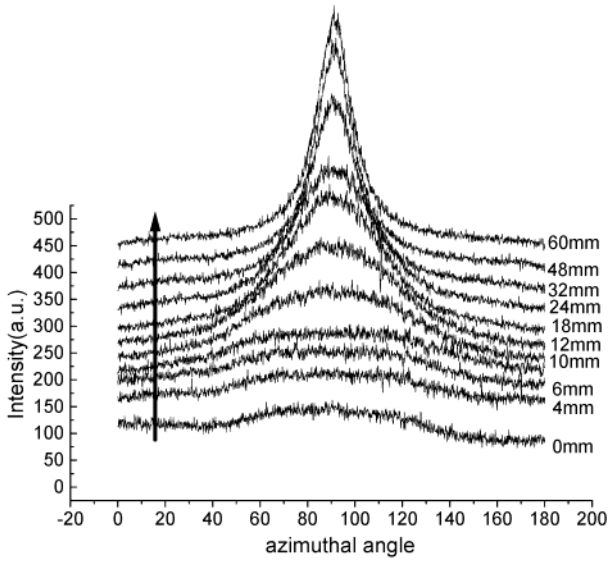

Figure 11. Azimuthal scans of (200) reflection of PEMA at various strains.

tion of crystallinity in PEMA/20A and PEMA/SiO_2 is similar to each other, the extent of lamellar fragmentation in PEMA/20A is less than that of PEMA/SiO_2.

Orientation Order Parameter (*S*) with Strain. The evidence for the chain slip is supported first by the onset of martensitic transformation at the first yield point.[21] Second, the rapid orientation of the orthorhombic (200) reflection, which we have shown to begin at the first yield point, can be related to (110) twinning followed by (100)[001] chain slip.[45] The molecular orientation is calculated by the following equation from the distribution of (200) peak intensity as a function of azimuthal angle:

$$S = \frac{3}{2}\langle\cos^2\beta\rangle - \frac{1}{2} = \frac{\int I|\sin\beta|\left(\frac{3}{2}\cos^2\beta - \frac{1}{2}\right)\mathrm{d}\beta}{\int I|\sin\beta|\,\mathrm{d}\beta} \quad (1)$$

where β is the azimuthal angle between the axis of a molecular segment and the machine direction of sample and I is the scattering intensity of the (200) reflection at the corresponding angles. From the meridian scan, appropriate background corrections are made. These corrections are necessary to account for an isotropic fraction of the material, which produces a genuine intensity at the same diffraction angle that is independent of azimuth.[46] Figure 11 shows azimuthal scans around the (200) reflection of PEMA. PEMA/20A and PEMA/SiO_2 show very similar azimuthal patterns with that of PEMA. The curve shows a very low degree of crystallite orientation until the strain reaches 10 mm. Figure 12 shows the orientation order parameter of (200) reflection as a function of strain, which is calculated on the basis of eq 1. Before the strain reaches 10 mm, PEMA/20A shows slightly higher orientation order than the other two samples. It may be associated with the presence of oriented silicates, which has occurred during the compression molding of PEMA/20A. The polymer chains may be easily oriented when the silicate particles are oriented under the molding pressure. It is known that the silicate also plays a role as a nucleating agent in the matrix.[29] The local structure and orientation of lamellae near the silicate has been well described

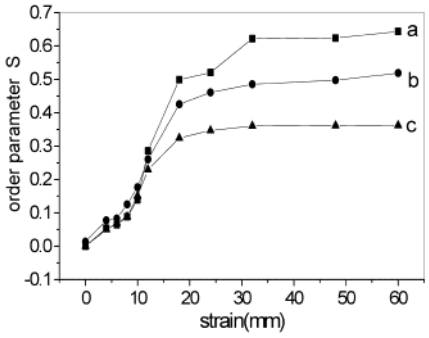

Figure 12. Orientation order parameter (*S*) vs strain: (a) PEMA, (b) PEMA/20A, (c) PEMA/SiO_2.

in other reports.[42,47,48] The lamellae in PEMA/20A may be arranged parallel to each other on the surface of silicate layers by nucleation effect.[47,48] On the contrary the SiO_2 particles of an isotropic shape cannot be oriented as the silicate particles do during the compression molding under pressure. Consequently, the degree of lamellae orientation near the SiO_2 particles is not greatly different from that of the pure PEMA. However, the PEMA shows a higher orientation than the others beyond the strain of 15 mm, which is the second yield point. It is conceivable that the orientation development upon stretching is affected by the presence of silicate, SiO_2, or the cavities. While PEMA/20A shows a lower degree of orientation than PEMA at the strains beyond 15 mm, it still shows a higher orientation than PEMA/SiO_2. It seems that layered silicates dispersed in the polymer matrix are inhibiting the orientation of chains but not as great as SiO_2 does. As discussed previously (Figure 5b), the silicates align themselves parallel to the drawing direction. Each layer thickness of silicate is supposed to be very thin in an exfoliated situation. Consequently, the inhibition of chain orientation by the oriented thin silicates is relatively less effective than that of large spherical SiO_2 particles. In PEMA/SiO_2, we also noted cavities formed during the tensile deformation. The sizes of cavities are in the range of several microns or more, as shown in Figure 4b. It is speculated that the polymer chains near the SiO_2 particles or cavities are hard to orient themselves in the direction parallel to tensile extension over the large spherical SiO_2 particles or the cavities.

Conclusions

PEMA/20A and PEMA/SiO_2 composites were prepared. TEM and X-ray scattering results confirmed the exfoliated state in PEMA/20A while PEMA/SiO_2 showed large aggregates of SiO_2 particles in the PEMA matrix. Upon cold drawing of the composites, PEMA/20A showed the orientation of silicates and a strong interfacial adhesion between the silicates and PEMA matrix. But in PEMA/SiO_2 extensive amount of large cavities were formed, demonstrating the poor interfacial adhesion between large SiO_2 particles and PEMA. The exfoliated silicates and SiO_2 aggregates both affect the crystallographic deformation of PEMA matrix during the tensile deformation. The pure PEMA showed the larger change in crystallinity and the higher chain orientation than the two composites. Martensitic transformation is observed approximately at the same strain level in all three samples. Even though similar crystallinity changes were observed during the deformation of PEMA/20A and PEMA/SiO_2, less fragmentation of crystal lamellae is

found in PEMA/20A. The dispersed particles appear to inhibit the orientation of lamellae by the tensile drawing. The large spherical SiO_2 aggregates and cavities are found to be more effective in inhibiting the orientation of lamellae in the tensile direction than the exfoliated thin silicate layers.

References and Notes

(1) Messersmith, P. B.; Giannelis, E. P. *J. Polym. Sci., Part A: Polym. Chem.* **1995**, *33*, 1047.
(2) Usuki, A.; Kawasumi, T.; Kojima, M.; Fukushima, Y.; Okada, A.; Kurauchi, T.; Kamigaito, O. *J. Mater. Res.* **1993**, *8*, 1179.
(3) Kojima, Y.; Usuki, A.; Kawasumi, M.; Fukushima, Y.; Okada, A.; Kurauchi, T.; Kamigaito, O. *J. Mater. Res.* **1993**, *8*, 1185.
(4) Yano, K.; Usuki, A.; Okada, A.; Kurauchi, T.; Kamigato, O. *J. Polym. Sci., Part A: Polym. Chem.* **1993**, *31*, 2493.
(5) Vaia, R. A.; Jandt, K. D.; Kramer, E. J.; Giannelis, E. P. *Macromolecules* **1995**, *28*, 8080.
(6) Biasci, L.; Aglietto, M.; Ruggeri, G.; Ciardelli, G. F. *Polymer* **1994**, *35*, 3296.
(7) Giannelis, E. P. *Adv. Mater.* **1996**, *8*, 29.
(8) Wang, Z.; Piannavaia, T. J. *Chem. Mater.* **1998**, *10*, 3769.
(9) Dagani, R. *Chem. Eng. News* **1999**, *77*, 25.
(10) Hudson, S. D. US5910523A.
(11) Inoue, H.; Hosokawa, T. EP 0807659A1.
(12) Kurokawa, Y.; Yasuda, H.; Oya, A. *J. Mater. Sci., Lett.* **1996**, *15*, 1481.
(13) Kurokawa, Y.; Yasuda, H.; Oya, A. *J. Mater. Sci., Lett.* **1997**, *16*, 1670.
(14) Oya, A.; Kurokawa, Y.; Yasuda, H. *J. Mater. Sci.* **2000**, *35*, 1045.
(15) Usuki, A.; Kato, M.; Okada, A.; Kuraushi, T. *J. Appl. Polym. Sci.* **1997**, *63*, 137.
(16) Kato, M.; Usuki, A.; Okada, A. *J. Appl. Polym. Sci.* **1997**, *66*, 1781.
(17) Kawasumi, M.; Hasegawa, N.; Kato, M.; Usuki, A.; Okada, A. *Macromolecules* **1997**, *30*, 6333.
(18) Hasegawa, N.; Kawasumi, M.; Kato, M.; Usuki, A.; Okada, A. *J. Appl. Polym. Sci.* **1998**, *67*, 87.
(19) Wang, K. H.; Choi, M. H.; Koo, C. M.; Choi, Y. S.; Chung, I. J. *Polymer* **2001**, *42*, 9819.
(20) Butler, M. F.; Donald, A. M.; Bras, W.; Mant, G. R.; Derbyshire, G. E.; Ryan, A. J. *Macromolecules* **1995**, *28*, 6383.
(21) Butler, M. F.; Donald, A. D.; Ryan, A. J. *Polymer* **1997**, *38*, 5521.
(22) Butler, M. F.; Donald, A. D.; Ryan, A. J. *Polymer* **1998**, *39*, 39.
(23) Vickers, M. E.; Fischer, H. *Polymer* **1995**, *36*, 2667.
(24) Muratoglu, O. K.; Argon, A. S.; Cohen, R. E.; Weinberg, M. *Polymer* **1995**, *36*, 921.
(25) Lin, L.; Argon, A. S. *Macromolecules* **1992**, *25*, 4011.
(26) Barczak, Z.; Argon, A. S.; Cohen, R. E. *Macromolecules* **1992**, *25*, 5036.
(27) Popli, R.; Mandelkern, L. *J. Polym. Sci., Polym. Phys. Ed.* **1987**, *25*, 441.
(28) Lucas, J. C.; Failla, M. D.; Smith, F. L.; Mandelkern, L. *Polym. Eng. Sci.* **1995**, *36*, 1117.
(29) Wang, K. H.; Choi, M. H.; Koo, C. M.; Xu, M.; Chung, I. J.; Jang, M. C.; Choi, S. W.; Song, H. H. *J. Polym. Sci., Part B: Polym. Phys.*, in press.
(30) Liu, Z. H.; Wu, L. X.; Kwok, K. W.; Zhu, X. G.; Qi, Z. N.; Choy, C. L.; Wang, F. S. *Polymer* **2001**, *42*, 1719.
(31) Dompas, D.; Groenninckx, G. *Polymer* **1994**, *35*, 4743.
(32) Dompas, D.; Groenninckx, G.; Isogawa, M.; Hasegawa, T.; Kadokura, M. *Polymer* **1995**, *36*, 437.
(33) Brooks, N. W.; Duckett, R. A.; Ward, I. M. *Polymer* **1992**, *33*, 1872.
(34) Brooks, N. W.; Unwin, A. P.; Duckett, R. A.; Ward, I. M. *J. Macromol. Sci., Phys.* **1995**, *B34*, 29.
(35) Lin, L.; Argon, A. S. *J. Mater. Sci.* **1971**, *29*, 294.
(36) Bowden, P. B.; Young, R. J. *J. Mater. Sci.* **1974**, *9*, 2034.
(37) Lu, X.; Wang, X.; Brown, N. *J. Mater. Sci.* **1988**, *23*, 643.
(38) Zhou, Z.; Brown, N. *Polymer* **1994**, *35*, 619.
(39) Kornmann, X.; Lindberg, H.; Berglund, L. A. *Polymer* **2001**, *42*, 1303.
(40) Earley, J. W.; Osthaus, B. B.; Milne, I. H. *Am. Mineral.* **1953**, *38*, 707.
(41) Vaia, R. A.; Vasudevan, S.; Krawiec, W.; Gscanlon, L. G.; Giannelis, E. P. *Adv. Mater.* **1995**, *2*, 154.
(42) Kim, G. M.; Lee, D. H.; Hoffmann, B.; Kressler, J.; Stoppelmann, G. *Polymer* **2001**, *42*, 1095.
(43) Cullity, B. D. *Elements of X-ray Diffraction*, 2nd ed.; Addison-Wesley: Reading, MA, 1978; p 102.
(44) Peterlin, A. *J. Mater. Sci.* **1971**, *6*, 490.
(45) Krause, S. J.; Hosford, W. F. I. *J. Polym. Sci., Polym. Sci. Ed.* **1989**, *27*, 1853.
(46) Davidson, J. A.; Jung, H. T.; Hudson, S. D.; Percec, S. *Polymer* **2000**, *41*, 3357.
(47) Jeon, H. G.; Jung, H. T.; Lee, S. W.; Hudson, S. D. *Polym. Bull. (Berlin)* **1998**, *41*, 107.
(48) Nam, P. H.; Maiti, P.; Okamoto, M.; Kotaka, T.; Hasegawa, N.; Usuki, A. *Polymer* **2001**, *42*, 9633.

MA020165N